# Influences of twist boundaries on optical effects: *Ab initio* studies of the deep ultraviolet nonlinear optical crystal KBe<sub>2</sub>BO<sub>3</sub>F<sub>2</sub>

Z. S. Lin, <sup>1,a)</sup> Lei Bai, <sup>1</sup> Lijuan Liu, <sup>1</sup> M. H. Lee, <sup>2</sup> J. Xu, <sup>3</sup> Xiaoyang Wang, <sup>1</sup> and C. T. Chen <sup>1</sup> Beijing Center for Crystal R&D, Key Laboratory of Functional Crystals and Laser Technology, Technical Institute of Physics and Chemistry, Chinese Academy of Sciences, P. O. Box 2711, Beijing 100190, China <sup>2</sup>Department of Physics, Tamkang University, Tamsui, Taipei 25137, Taiwan <sup>3</sup>Department of Physics, Renmin University of China, Beijing 100872, China

(Received 14 November 2010; accepted 19 February 2011; published online 11 April 2011)

Twist boundaries in the deep-UV nonlinear optical crystal KBe<sub>2</sub>BO<sub>3</sub>F<sub>2</sub> (KBBF) are studied through first-principles calculations. It was found that the optical qualities and the capability for second-harmonic generation (SHG) in KBBF obtained from the different single-crystal growth methods are very different. These properties are associated with the presence of defects. Our studies demonstrate that the (0001) twist boundaries in KBBF are easily formed due to the quite weak interaction between the in-plane layers. These grain boundaries have very small influences on the modifications of the UV optical absorption edge and the refractive indices in KBBF. However, the SHG conversion efficiency in KBBF can be significantly deteriorated as the (0001) twist boundaries occur, so it is necessary to eliminate these twist boundaries during the single-crystal growth processes. Our theoretical results are consistent with experimental observations. © 2011 American Institute of Physics. [doi:10.1063/1.3569836]

## I. INTRODUCTION

KBe<sub>2</sub>BO<sub>3</sub>F<sub>2</sub> (KBBF) crystal is so far the sole nonlinear optical (NLO) crystal that can break the "200-nm wall" in the deep-ultraviolet (DUV) spectrum using direct second-harmonic generation (SHG), hence, it has important applications in super-high-resolution laser photoemission spectrography and photolithography.<sup>2</sup> However, KBBF grows thin and platelike (only 3~4 mm thickness along the c-axis) by the standard flux crystal-growth method, 3,4 which severely hinders its applications. Recently, a different crystal-growth method, i.e., the hydrothermal method, has been employed<sup>5,6</sup> and KBBF crystals with thicknesses approaching 1 cm have been achieved. However, the optical properties of hydrothermal-grown (H-) KBBF crystals are quite different from those of flux-grown (F-) crystals: the optical uniformity in the former crystals is much worse than in the latter and, more evidently, the SHG capability in the H-KBBF crystals is much deteriorated; typically its conversion efficiency is several times lower than in the F-crystals. All these phenomena suggest that the H-KBBF crystals might not be suitable for DUV SHG at the current stage of development. Therefore, it is important to elucidate the mechanisms that cause these optical differences in the H- and F-KBBF crystals, which would be of great benefit to the improvement of optical performance in H-KBBF.

Detailed structural comparisons between the H-KBBF and F-KBBF have been performed by Yu *et al.*<sup>7</sup> They found that the x-ray diffraction (XRD) patterns in the H-KBBF crystal are almost identical with those in the F-KBBF, despite that three very small peaks occur in the former's XRD spectrum. This indicates that the KBBF

crystals obtained by the different growth methods possess very similar basic structural features. Meanwhile, there is no evident distinction between the constituent chemical element content in the F- and H-KBBF crystals, suggesting that atomic vacancies or impurities are not the main factors in producing the optical difference. Further transmission electron microscope measurements demonstrated that the H-KBBF crystal has many more stacking faults, such as dislocations, grain boundaries, and twins, compared to the F-KBBF. Therefore, Yu et al. concluded that the optical differences mainly resulted from the presence of structural defects in KBBF. However, it is still unclear from experimental measurements how the defects affect the optical properties in KBBF, owing to the complicated crystalline environments. These complicated situations can actually be simplified by adopting another research strategy, i.e., atomic modeling, which is anticipated to provide insight into the influences of respective defects in an effective and precise way. We believe that these theoretical studies can be widely applied to other nonlinear optical crystals equally.

The space group of KBBF is R32 [point group D3 (32)], belonging to the uniaxial class, with dimensions of a=b=4.427(4) Å, c=18.744(9) Å, and a Z value of 3. In each unit cell, there are three  $(Be_2F_2BO_3)_{n\to\infty}$  two-dimensional (2D) layers perpendicular to the c-axis [Fig. 1(a)], in which all planar  $(BO_3)$  groups are aligned in the same orientation [comparison of the blue (dark gray) and green (light gray) triangles in Fig. 1(b)]. In each in-plane layer three terminal O atoms of all  $(BO_3)$  groups link with the nearest neighbor, while each Be atom links with a F atom outside of the layer. Accordingly, one may easily find that one of the simplest stacking faults in KBBF is the twist grain boundary by rotating the  $(Be_2F_2BO_3)$  layer about the c-axis, forming the (0001) twist boundary. Indeed this type of grain

a) Author to whom correspondence should be addressed. Electronic mail: zslin@mail.ipc.ac.cn.

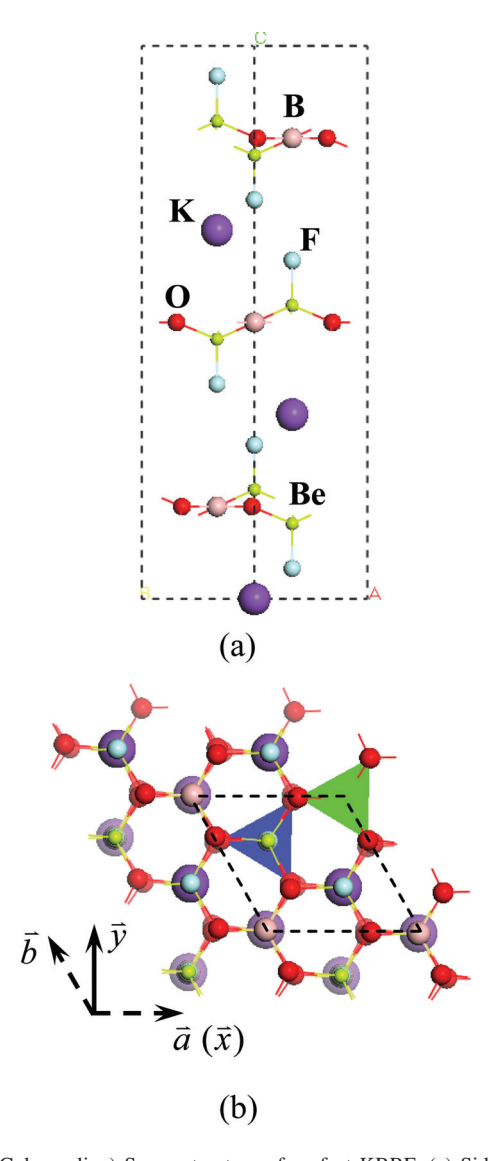


FIG. 1. (Color online) Space structure of perfect KBBF. (a) Side view of the unit cell. (b) Depth-cue top view of detailed layer structure. The *a-b* vectors indicate the crystallographic axes, and the *x-y* vectors indicate the optical dielectric axes. The *c*-axis (or *z*-axis) is normal to the paper plane and points to the outside. Green (light gray) and blue (dark gray) triangles represent the planer (BO<sub>3</sub>) groups in the outmost and deeper layers, respectively, as in all the following figures.

boundary is one of the main stacking faults observed in the H-crystals, much more commonly than in the F-crystals. Therefore, it is important to understand the influences of the (0001) twist boundaries on the modifications of the optical effects in KBBF.

In this work, the structural features of the (0001) twist boundaries present in KBBF are studied, and their influences on optical properties are investigated using first-principles computational approaches. It is found that the (0001) twist boundaries are indeed relatively easy to form because of the quite small twist boundary energy, and their influence on the modifications of both the optical UV absorption edge and linear optical effects in the KBBF crystals is only in a very tiny degree. However, the SHG capability in KBBF can be heavily deteriorated by the (0001) twist boundaries since the microscopic structural units are out of alignment therein.

## II. (0001) TWIST BOUNDARIES IN KBBF

In a hexagonal lattice the (0001) twist boundary is formed by rotating the a-b layers about the c-axis with an angle (e.g.,  $\lambda$ ), so the corresponding rotation matrix is:

$$\begin{bmatrix} \cos \lambda - \frac{\sqrt{3}}{3} \sin \lambda & \frac{2\sqrt{3}}{3} \sin \lambda & 0\\ -\frac{2\sqrt{3}}{3} \sin \lambda & \cos \lambda + \frac{\sqrt{3}}{3} \sin \lambda & 0\\ 0 & 0 & 1 \end{bmatrix}. \tag{1}$$

However, the allowed rotation angle  $\lambda$  is not arbitrary if there is no internal stress and strain present in the lattice. The N times of the rotated lattice constants must be equal to the M times of the underlayer lattice constants, where N and M are integers. This means that this rotation matrix must be always rational, so we are looking for three integers A, B, and C which satisfy the relation of  $A^2 = B^2 + 3C^2$ , i.e.,  $\sin \lambda = \sqrt{3}(C/A)$  and  $\cos \lambda = B/A$ . Furthermore, the least common integer in the denominator of the matrix is the degree of fit  $(\Sigma)$ , which is the reciprocal of the ratio of coincidence sites to the total number of sites.

From the above analysis, one may easily find that the (0001) twist boundaries rotated by  $\lambda$  and  $60^{\circ} \pm \lambda$  must have the same degree of fit ( $\Sigma$ ) in hexagonal lattices. Table I lists the allowed rotated angles  $\lambda$  of the lattice vectors in the a-b (or x-y) plane with respect to the  $\Sigma$  increases. Here we only consider the first three  $\Sigma$ s in detail due to the limits of computational resources, but the main physical and optical properties remain for any other (0001) twist boundary in larger scale.

In KBBF, each unit cell contains three (Be<sub>2</sub>F<sub>2</sub>BO<sub>3</sub>) 2D layers. Therefore, in our studied models the twist boundary can be created by dividing the structure along the c-axis and rotating one third of the crystal with respect to the remainder about the c-axis in a supercell. Here we ignore any internal stress and strain inside the KBBF lattices, and assume that the twist boundary is independent of the translation states along the a-b plane. Figures 2, 3, and 4 show the geometries for the  $\Sigma$  1,  $\Sigma$  7, and  $\Sigma$  13 (0001) twist boundaries in KBBF, respectively. The simplest twist boundary is created by rotating the three O atoms only around the central B atom in each (BO<sub>3</sub>) group by 60.0° at the boundary while keeping the other atomic positions unchanged, forming a so-called  $\Sigma$  1 (BO<sub>3</sub>-R60.0) boundary [Fig. 2(a)]. The other type of  $\Sigma$  1 boundary is shown in Fig. 2(b), in which all atoms at the boundary are rotated by  $60.0^{\circ}$  about the *c*-axis [ $\Sigma$  1 (*R*60.0)]. Figures 3(a), 3(b), and 3(c) show the geometries for the  $\Sigma$  7

TABLE I. Allowed rotated angles  $\theta$  (0°  $\leq \theta \leq 90^{\circ}$ ) of the lattice vectors in the a-b (or x-y) plane as the twist boundaries formed in hexagonal cell. (Unit: degree).

Σ	1	7	13	19	31	37	
Rotation	0.0	21.8	27.8	13.2	17.9	9.4	
		38.2	32.2	46.8	42.1	50.6	
	60.0	81.8	87.8	73.2	77.9	69.4	

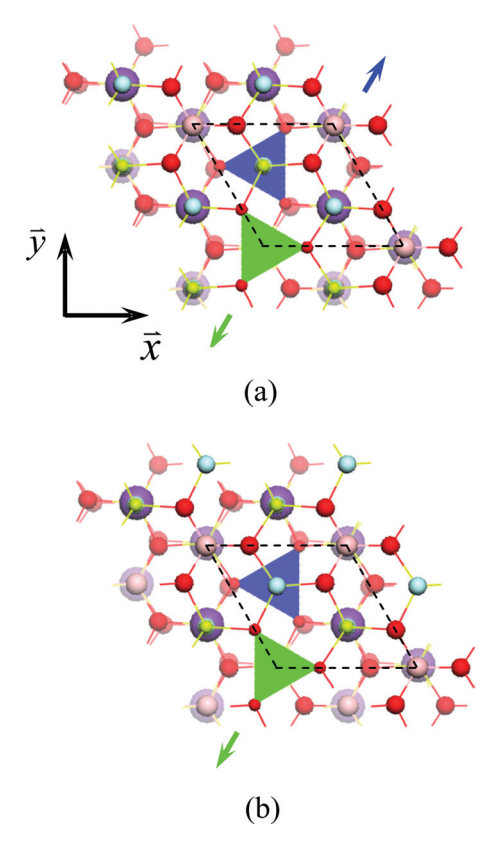


FIG. 2. (Color online) Top view of the  $\Sigma$  1 twist boundary in KBBF. (a) BO3-R60.0. (b) R60.0. It is worth noting that there are three orientations for each (BO<sub>3</sub>) group, but they are equivalent to one another due to the D3 point group symmetry. An orientation of the rotated (BO<sub>3</sub>) groups is indicated by the green (light gray) arrow, while that of the original (BO<sub>3</sub>) groups is indicated by the blue (dark gray) arrow. The dashed box represents a supercell in which the twist boundary is formed.

twist boundaries with the rotated angles of  $21.8^{\circ}$  [ $\Sigma$  7 (R21.8)],  $38.2^{\circ}$  [ $\Sigma$  7 (R38.2)] and  $81.8^{\circ}$  [ $\Sigma$  7 (R81.8)], respectively. The  $\Sigma$  13 twist boundaries with rotated angles of  $27.8^{\circ}$  [ $\Sigma$  13 (R27.8)],  $32.2^{\circ}$  [ $\Sigma$  13(R32.2)] and  $81.8^{\circ}$  [ $\Sigma$  13(R81.8)] are displayed in Fig. 4. Clearly, the orientation of the (BO<sub>3</sub>) groups [green (light gray) arrows in Figs. 2, 3, and 4] at the  $R(\lambda)$  twist boundary is in mirror symmetry about the y-z plane with that at the  $R(60^{\circ} - \lambda)$  boundary, but is antiparallel to the orientation of the  $R(60^{\circ} + \lambda)$  boundary, due to the restriction of the point group symmetry in KBBF. These structural modifications are expected to have significant influences on the optical properties, especially the SHG effects in KBBF, which are dominantly determined by the (BO<sub>3</sub>) group.  $^{9.10}$ 

## **III. COMPUTATIONAL METHOD**

The (0001) twist boundaries in KBBF are studied by the plane-wave pseudopotential method. <sup>11</sup> The CASTEP program <sup>12</sup> is employed to perform the optimized geometries and the electronic structure calculations. Ultrasoft pseudopotentials <sup>13</sup> are used with the 1s electrons for beryllium, boron, and oxygen treated as core electrons. For potassium, 3s, 3p, and 4s electrons are chosen as the valence electrons. A high kineticenergy cutoff of 500 eV and the generalized-gradient

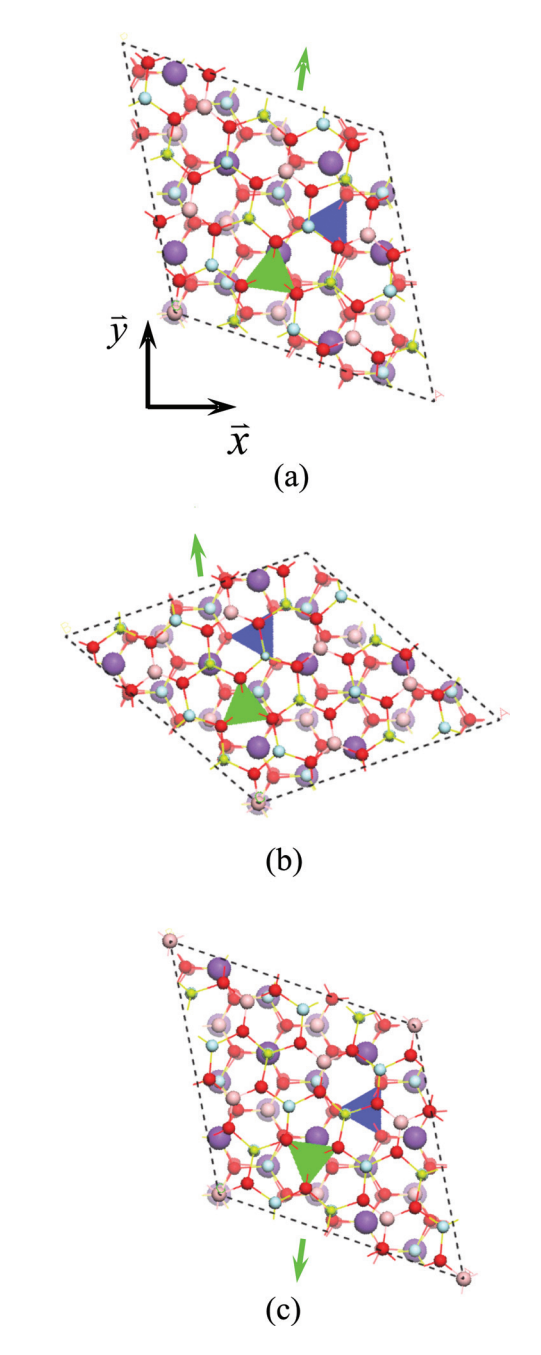


FIG. 3. (Color online) Top view of the  $\Sigma$  7 twist boundary in KBBF. (a) R21.8. (b) R38.2. (c) R81.8. Symbol conventions are as for the preceding figures.

approximation (GGA) with the Perdew, Burke, and Ernzerhof exchange-correlation functional  $^{14}$  are chosen for all the calculations. Monkhorst–Pack  $^{15}$  k-point meshes with a density of at least ( $7 \times 7 \times 1$ ) points in the Brillouin zone of the KBBF unit cell are used. The atomic positions are relaxed by the Broyden, Fletcher, Goldfarb, and Shannon minimizer.  $^{16}$  The convergence thresholds between optimization cycles for energy change, maximum force, and maximum displacement are set as  $10^{-5}$  eV/atom, 0.03 eV/Å, and 0.001 Å, respectively. The optimization terminates when all of these criteria are satisfied.

The relative stabilities of the twist boundaries are determined by the grain boundary energy  $\sigma$ , and defined by

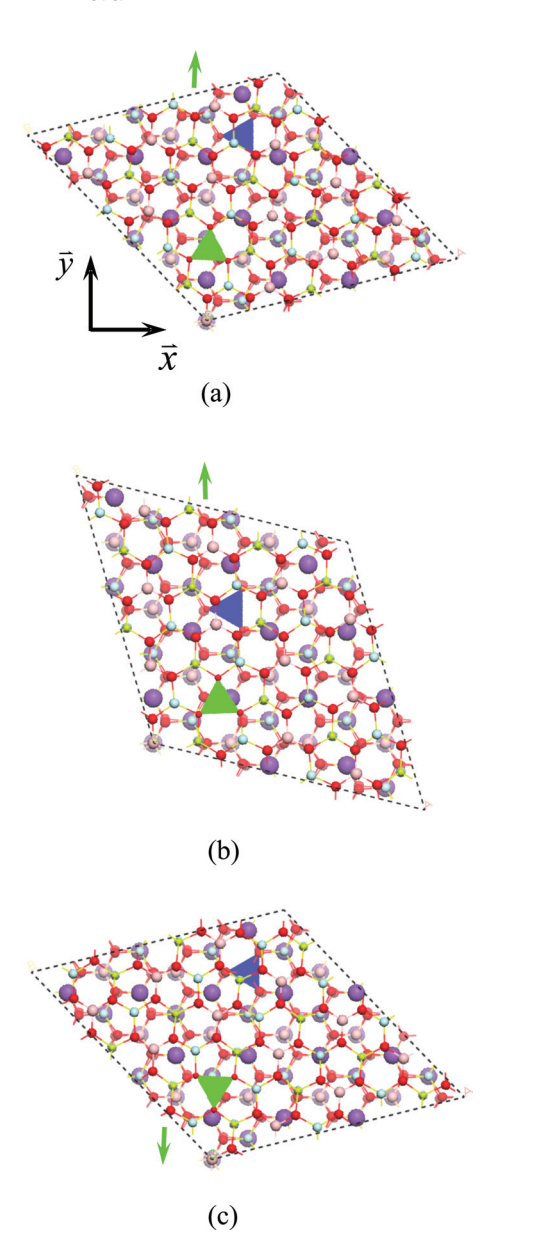


FIG. 4. (Color online) Top view of the  $\Sigma$  13 twist boundary in KBBF. (a) R27.8. (b) R32.2. (c) R87.8. Symbol conventions are as for the preceding figures.

$$\sigma = (E_{gb} - NE_0)/2A \tag{2}$$

where  $E_{gb}$  is the total energy of the supercell containing the grain boundary,  $E_0$  is the total energy of a perfect KBBF unit cell, N is the degree of fit  $\Sigma$ , and A is the twist boundary area. The factor of 1/2 comes from the fact that two grain boundaries are present in the supercell.

On the basis of the relaxed geometries, the electronic band structures and the optical properties of KBBF containing the grain boundaries are obtained. The detailed formulae for calculating the linear and nonlinear optical coefficients are given in Ref. 9.

## IV. RESULTS AND DISCUSSION

The calculated twist boundary energies in KBBF are listed in Table II. It is clear that the value increases as the

TABLE II. Calculated boundary energies and energy band gaps of the defected KBBF crystals with various twist boundaries. Meanwhile, the corresponding UV optical absorption edges are also listed for clarification purposes. To obtain these optical edges, a scissors operator, 2.44 eV, is adopted.

Boundar	у	Boundary energy (meV/Ų)	Energy bandgap (eV)	UV absorption edge (nm)
Perfect KBBF		_	5.83	150.0 <sup>a</sup>
$\Sigma$ 1	$BO_3_R60.0$	$\sim 0$	5.82	150.2
	R60.0	15	5.84	149.8
Σ7	R21.8	26	5.83	150.0
	R38.2	26	5.81	150.4
	R81.8	27	5.80	150.5
Σ 13	R27.8	34	5.73	151.8
	R32.8	35	5.75	151.5
	R87.8	34	5.76	151.3

<sup>&</sup>lt;sup>a</sup>Reference 4.

degree of fit  $\Sigma$  increases, indicating that boundaries with smaller  $\Sigma$  form easier. In particular, for the  $\Sigma$  1 (BO<sub>3</sub>-R60.0) twist boundary the 60° rotation of the (BO<sub>3</sub>) groups in the a-b plane almost does nothing to the modification of the total energy of the system and the calculated boundary energy is negligibly small, so this boundary is the most favored in KBBF. Indeed, very current structural measurements have confirmed that the occurrence of new peaks in the XRD spectrum is due to the formation of the  $\Sigma$  1 (BO<sub>3</sub>-R60.0) twist boundary in KBBF.<sup>17</sup> In addition, with the increase of the  $\Sigma$  the twist boundary energies are quickly converged to a quite small value ( $< 50 \text{ meV/Å}^2$ ). This can be understood by the fact that the distance between adjacent in-plane layers in KBBF is quite large, being 6.25 Å, so only very weak bonding exists between the layers. However, in practice (0001) twist boundaries may not be easy to form on a larger scale considering the restriction of the surrounding crystalline environments, and they would be evolved further to be the more disordered defects.

On the other hand, it should be noted that our above calculations are only based on the static atomic configurations at absolute zero. In practice, the formation of twist boundaries is strongly dependent on the thermodynamic environments. To estimate the energy barrier of the twist boundary formed from the original perfect lattice, we use the complete LST/QST algorithm<sup>18</sup> to perform the transition state searches, and find that the transition energy between the perfect and twist structure is very high. For example, even for the  $\Sigma$  1 (BO<sub>3</sub>-R60.0) twist boundary the transition energy is about 3.0 eV per in-plane unit cell. Therefore, one may explain the reason why the occurrence possibility of twist boundaries (and other defects) in the H-KBBF is much higher than in the F-KBBF as follows. It is well known that the perfection of an as-grown crystal is controlled by the interplay of the deposition and diffusion of adsorbed atoms on the crystal surface. 19 If deposition is slower than diffusion, growth would occur close to equilibrium conditions, but if deposition is faster than diffusion, then the pattern of growth is essentially determined by individual processes, notably those leading to metastable structures. Accordingly, in the hydrothermal growth autoclave the transportation of growth solutes onto the crystal surface is quite quick, and the adsorbed atoms can easily produce some metastable patterns such as grain boundaries, dislocations, or twins, which are difficult to recover to the minimum energy (perfect) configuration due to the high energy barriers; while in the flux growth process the growth environments can be subtly controlled so that the occurrence of stacking faults is greatly reduced.

It is known that the bandgap calculated by GGA, a ground state theory, is in general smaller than the experimental data for the wide-bandgap insulator. However, our previous studies have demonstrated that actually the relative magnitude of calculated bandgaps can be used to compare the UV absorption edge in borate NLO crystals. 10 The calculated energy bandgaps for various twist boundaries in KBBF are shown in Table II. It is clear that the energy bandgap of KBBF tends to be smaller as the degree of fit for the twist boundaries becomes larger, but the narrowing magnitude is very small. For instance, the calculated UV absorption edge for the  $\Sigma$  13 twist boundaries is red shifted only about 1.5 nm compared to the perfect KBBF. The detailed electronic structure analysis shows that this narrow a bandgap is because some 2p orbitals of the fluorine atoms at the boundary occupy the valence band maximum and slightly affect the bandgap.

The calculated refractive indices in several wavelengths for various twist boundaries are shown in Table III, from which several conclusions can be obtained: (1) The calculated refractive indices for the perfect KBBF crystal are in good agreement with the experimental values, indicating the reliability of the first-principles methods used. (2) The KBBF crystal keeps as a uniaxial crystal form no matter how the twist boundaries rotate about the c- (or z-) axis. This is because in a uniaxial crystal the linear optical response of the a-b (or x-y) plane to the incident radiation is isotropic and independent of its rotation about the optical z-axis. (3) Both the refractive indices and birefringence in the perfect KBBF crystal are changed as the twist boundaries [except  $\Sigma$  1 (BO<sub>3</sub>-R60.0)] are formed. However, the modifications of the linear optical constants are rather small, typically less than 0.02. Therefore, the much worse optical uniformity in the H-KBBF compared to the F-KBBF may be attributed to the existence of other types of defects, e.g., dislocations and twins. The relevant studies are under investigation.

Table IV lists the nonzero SHG coefficients in KBBF containing various twist boundaries. The perfect KBBF belongs to the space group R32, so it has only two nonzero  $d_{ij}$  coefficients, i.e.,  $d_{11} = -d_{12}$  and  $d_{14}$ , and the experimental values are  $d_{11} = 0.47$  pm/V and  $d_{14} \sim 0.4$  The calculated values in this work are  $d_{11} = 0.430$  pm/V and  $d_{14} = 0$ , in very good agreement with the experimental measurements, and slightly better than the previous values  $(d_{11} = 0.351 \text{ pm/V})^9$  using the local density approximation and norm-conserving pseudopotentials. As the  $\Sigma$  1 twist boundaries are created the  $d_{11}$  coefficient becomes much smaller, only about one third of the original value in the perfect KBBF. For the other twist boundaries two more nonzero SHG coefficients  $d_{21}$  and  $d_{22}$ 

TABLE III. Comparison of the refractive indices in several wavelengths for various twist boundaries.  $n_o$  (=  $n_x$  and  $n_y$ ) and  $n_e$  (=  $n_z$ ) are the refractive indices for the ordinary and extraordinary radiation, respectively, and  $\Delta n$  is the birefringence.

			Refractive indices in several wavelengths				
Wavelength (nm)		656.2	578.0	491.6	404.7		
KBBF (Exp.) <sup>a</sup> $n_0$		1.4788	1.4811	1.4851	1.4915		
		$n_{\rm e}$	1.3954	1.3968	1.3993	1.4035	
		$\Delta n$	0.0834	0.0843	0.0858	0.0880	
KBBF (Cal.) $n_{\rm o}$		1.4718	1.4735	1.4767	1.4822		
		$n_{\rm e}$	1.4046	1.4059	1.4081	1.4119	
		$\Delta n$	0.0672	0.0676	0.0686	0.0703	
$\Sigma 1$	BO3_ <i>R</i> 60.0	$n_{\rm o}$	1.4717	1.4735	1.4767	1.4822	
		$n_{\rm e}$	1.4045	1.4058	1.4080	1.4118	
		$\Delta n$	0.0672	0.0677	0.0687	0.0704	
	R60.0	$n_{\rm o}$	1.4843	1.4859	1.4887	1.4836	
		$n_{\rm e}$	1.4215	1.4228	1.4250	1.4188	
		$\Delta n$	0.0628	0.0631	0.0637	0.0648	
$\Sigma 7$	R21.8	$n_{\rm o}$	1.4972	1.4988	1.5016	1.5064	
		$n_{\rm e}$	1.4441	1.4453	1.4475	1.4512	
		$\Delta n$	0.0531	0.0535	0.0541	0.0552	
	R38.2	$n_{\rm o}$	1.4969	1.4985	1.5012	1.5061	
		$n_{\rm e}$	1.4438	1.4450	1.4471	1.4509	
		$\Delta n$	0.0531	0.0535	0.0541	0.0552	
	R81.8	$n_{\rm o}$	1.4972	1.4988	1.5016	1.5064	
		$n_{\rm e}$	1.4440	1.4453	1.4474	1.4512	
		$\Delta n$	0.0532	0.0535	0.0542	0.0552	
$\Sigma 13$	R27.8	$n_{\rm o}$	1.4814	1.4830	1.4858	1.4907	
		$n_{\rm e}$	1.4282	1.4295	1.4316	1.4354	
		$\Delta n$	0.0532	0.0535	0.0542	0.0553	
	R32.2	$n_{\rm o}$	1.4815	1.4831	1.4859	1.4908	
		$n_{\rm e}$	1.4270	1.4282	1.4303	1.4341	
		$\Delta n$	0.0545	0.0549	0.0556	0.0567	
	R87.8	$n_{\rm o}$	1.4814	1.4830	1.4858	1.4907	
		$n_{\rm e}$	1.4268	1.4280	1.4302	1.4339	
		$\Delta n$	0.0546	0.0550	0.0556	0.0568	

<sup>&</sup>lt;sup>a</sup>Reference 4.

occur, and the  $d_{ij}$  coefficients satisfy the symmetry that  $d_{11} = -d_{12}$  and  $d_{22} = -d_{21}$ . All of the SHG coefficients are smaller than the  $d_{11}$  coefficient in the perfect KBBF.

Table IV also displays the calculated results from a semiempirical method called the anionic group theory,  $^{20}$  which provides a concise and substantial way to understand the mechanism of NLO effects in UV NLO crystals. According to the anionic group theory, the overall SHG coefficients  $d_{ijk}^{(2)}$  in a NLO crystal are the geometrical superpositions of the microscopic second-order susceptibilities of the anionic groups, and have nothing to do with the essentially spherical cations (e.g.,  $K^+$  cations in the case of KBBF). That is,

$$d_{ijk}^{(2)} = \frac{F}{N} \sum_{P} N_{P} \sum_{i'i'k'} \alpha_{ii'} \alpha_{jj'} \alpha_{kk'} d_{i'j'k'}^{(2)}$$
(3)

where F is the local field factor, V is the volume of a unit cell,  $N_P$  is the number of the pth anionic group in this unit cell, and  $\alpha_{ii'}$ ,  $\alpha_{jj'}$ , and  $\alpha_{kk'}$  are the direction cosines between the macroscopic coordinates of the crystal and the microscopic coordinates of the pth group.  $d_{i'j'k'}^{(2)}$  is the microscopic second-order susceptibility of the pth anionic group. Our

TABLE IV. Calculated non-zero SHG coefficients in KBBF with various twist boundaries. The values determined by the anionic group theory are listed in parentheses as comparisons (Unit: pm/V).

Boundary		$d_{11}$	$d_{12}$	$d_{21}$	$d_{22}$
	Perfect	0.430	-0.430	0.0	0.0
Σ 1	BO <sub>3</sub> _R60.0	0.143 (0.143)	-0.143(-0.143)	0.0 (0.0)	0.0 (0.0)
	R60.0	0.142 (0.143)	-0.142(-0.143)	0.0 (0.0)	0.0 (0.0)
Σ7	R21.8	0.340 (0.346)	-0.340(-0.346)	0.128 (0.130)	-0.128(-0.130)
	R38.2	0.223 (0.226)	-0.223 (-0.226)	0.130 (0.130)	-0.130(-0.130)
	R81.8	0.228 (0.226)	-0.228 (-0.226)	-0.120 (-0.130)	0.120 (0.130)
Σ 13	R27.8	0.292 (0.302)	-0.292(-0.302)	0.138 (0.142)	-0.138(-0.142)
	R32.8	0.260 (0.265)	-0.260(-0.265)	0.139 (0.142)	-0.139(-0.142)
	R87.8	0.259 (0.265)	-0.259(-0.265)	-0.138(-0.142)	0.138 (0.142)

previous studies have revealed that for borate UV NLO crystals the SHG effects are dominantly attributed to the anionic  $(BO_3)^{3-}$  groups, and are independent of the translation states of the  $(Be_2F_2BO_3)$  layer along the *a-b* plane. <sup>10</sup> Clearly, the values from the anionic group theory are in excellent agreement with those from the first-principles theory.

With the help of the anionic group theory, one may easily understand the structural origins of the SHG modifications in KBBF with respect to the twist boundaries as follows. In the perfect KBBF lattice all the (BO<sub>3</sub>)<sup>3-</sup> groups are aligned in the same orientation in the *a-b* planes [see Fig. 1(b)], so the geometrical superimposition of the microscopic  $d_{i'i'k'}^{(2)}$  of all  $(BO_3)^{3-}$  groups is scalar without any counteraction. Since in the present calculations three (Be<sub>2</sub>F<sub>2</sub>BO<sub>3</sub>) layers are employed in each supercell, the  $(BO_3)^{3-}$  groups in each layer exactly contribute one third of the overall SHG coefficients, i.e.,  $d_{111}^{1/3}$  (Perfect) = 1/3 $d_{11}$ (Perfect) = 0.143 pm/ V. As the  $\Sigma$  1 twist boundary models are created the rotated  $(BO_3)^{3-}$  groups are totally antiparallel to the original  $(BO_3)^{3-}$  groups [comparison of the green (light gray) and blue (dark gray) triangles in Fig. 2], and make a completely counteractive contribution to the overall SHG effects, so the coefficient  $d_{11}$  of the KBBF crystals having this type of twist boundaries is only one third of the original value. More generally, for the other (0001) twist boundaries the orientation of the rotated (BO<sub>3</sub>)<sup>3-</sup> group is no longer parallel or antiparallel to the others, and new nonzero SHG coefficients  $d_{222}^{1/3}$  $(=-d_{211}^{1/3})$  are generated. According to the geometry analysis in Sec. II, the orientation of the rotated  $(BO_3)^{3-}$  groups at the  $R(\lambda)$  twist boundary is always in the mirror symmetry about the y-z plane with that at the  $R(60^{\circ} - \lambda)$  boundary, but is in antiparallel orientation to that at the  $R(60^{\circ} + \lambda)$  boundary [comparison of the green (light gray) arrows shown in Figs. 2, 3, and 4, respectively]. Therefore, the projection of the corresponding orientation vectors of the rotated (BO<sub>3</sub>)<sup>3</sup>groups onto the x- or y-axes [i.e., the direction cosines  $\alpha$ 's in Eq. (3)] directly determines the SHG coefficients of the rotated layer, which must satisfy the following relation:

$$\begin{split} d_{111}^{1/3}(R(\lambda)) &= -d_{111}^{1/3}(R(60^{\circ} - \lambda)) = -d_{111}^{1/3}(R(60^{\circ} + \lambda)) \\ &= d_{111}^{1/3}(\operatorname{Perfect}) \times \cos 3\lambda \\ d_{222}^{1/3}(R(\lambda)) &= d_{222}^{1/3}(R(60^{\circ} - \lambda)) = -d_{222}^{1/3}(R(60^{\circ} + \lambda)) \\ &= -d_{111}^{1/3}(\operatorname{Perfect}) \times \sin 3\lambda \end{split} \tag{4}$$

Consequently, the overall SHG coefficients for the KBBF crystal containing the  $R(\lambda)$  twist boundary is:

$$\begin{aligned} d_{11}(R(\lambda)) &= 2d_{111}^{1/3}(\text{Perfect}) + d_{111}^{1/3}(R(\lambda)) \\ &= 1/3d_{11}(\text{Perfect}) \times (2 + \cos 3\lambda) = -d_{12}(R(\lambda)) \\ d_{22}(R(\lambda)) &= d_{222}^{1/3}(R(\lambda)) = 1/3d_{11}(\text{Perfect}) \\ &\times \sin 3\lambda = -d_{21}(R(\lambda)) \end{aligned} \tag{5}$$

It is worth mentioning that in the above calculations we only consider the twist boundary models in which each supercell contains three in-plane layers. In practice, the SHG coefficients in Eq. (5) are varied with respect to the number of layers employed and rotated in the atomic modeling. For instance, the SHG effects would vanish provided that an even number of the layers is present and one half are rotated by  $60^{\circ}$  with respect to the others in a supercell. Moreover, one may see that the SHG coefficient  $d_{11}$  is the largest as the orientations of all  $(BO_3)^{3-}$  groups are exactly parallel to one another in the case of perfect KBBF, and the value becomes smaller as long as the (0001) twist boundaries are created.

The SHG capability of a NLO crystal is directly determined by the effective  $d_{\text{eff}}$  coefficients, which are expressed for the perfect KBBF as follows:<sup>4</sup>

$$d_{11}\cos\theta\cos3\varphi \quad \text{(type-I)} d_{11}\cos^2\theta\sin3\varphi \quad \text{(type-II)}$$
 (6)

The  $d_{\rm eff}$  is maximum at  $\varphi=0^\circ$  for type-I phase-matching condition, while it is maximum at  $\varphi=30^\circ$  or  $90^\circ$  for type-II phase-matching condition. When the twist boundaries are formed, one more independent nonzero SHG coefficient  $d_{22}$  (=  $-d_{21}$ ) occur, and accordingly the effective  $d_{\rm eff}$  coefficients become:

$$\cos \theta(d_{11}(R(\lambda))\cos 3\varphi - d_{22}(R(\lambda))\sin 3\varphi) \quad \text{(type-I)}$$

$$\cos^2 \theta(d_{11}(R(\lambda))\sin 3\varphi + d_{22}(R(\lambda))\cos 3\varphi) \quad \text{(type-II)}$$
(7)

After some mathematic treatment one may easily find that the modified  $d_{\rm eff}$  coefficients [in Eq. (7)] are always smaller than the values [in Eq. (6)] in the perfect KBBF. Namely, the (0001) twist boundaries, no matter how they are rotated around the c- (or z-) axis, reduce the SHG efficiency in KBBF. Therefore, the occurrence of these structural defects,

with a much higher possibility in H-KBBF compared to F-KBBF, is the main factor in deteriorating the capability of SHG output in the former crystals, although other types of stacking faults such as tilt grain boundaries, dislocations, and twins may have some impacts as well.

## V. CONCLUSIONS

In this work, the (0001) twist boundaries present in KBBF have been studied, not only on their geometries, but also on their energetic and optical properties based on the first-principle density functional theory. It is found that the twist boundary is most likely to be the  $\Sigma$  1 (BO<sub>3</sub>-R60.0), confirmed by the current XRD data. The boundary energy increases as the degree of fit increases but is converged to a very low value due to the weak interaction between the a-b layers. The corresponding energy band gaps almost keep as the original value despite the influence of defect-induced states. The refractive indices and birefringence are also modified in a very tiny degree, and the uniaxial nature of the linear optical properties in KBBF remains. With the help of the anionic group theory it is further revealed that as the (0001) twist boundaries are present in KBBF, resulting in the microscopic NLO units going out of alignment, the SHG conversion efficiency definitely decreases, and in extreme cases the SHG effects vanish. In other words, the (0001) twist boundaries need to be eliminated in order to enhance the capability for producing SHG effects in KBBF. We believe that these theoretical understandings have great implications for improvement of the NLO performance in KBBF, and even in other optical crystals.

#### **ACKNOWLEDGMENTS**

This work was supported by the Special Foundation of the President of the Chinese Academy of Sciences and National Basic Research Project of China (No. 2010CB630701). MHL is grateful for the support from NSC (97-2112-M-032-004-MY2), NCHC and NCTS of Taiwan.

<sup>1</sup>R. D. Schaeffer and T. Hannon, Laser Focus World **37**, 115 (2001).

<sup>2</sup>D. Cyranoski, Nature **457**, 953 (2009).

<sup>3</sup>C. T. Chen, Y. Wang, Y. N. Xia, B. C. Wu, D. Y. Tang, K. C. Wu, W. R. Zeng, L. H. Yu, and L. F. Mei, J. Appl. Phys. 77, 2268 (1995).

<sup>4</sup>C. T. Chen, G. L. Wang, X. Y. Wang, and Z. Y. Xu, Appl. Phys. B **97**, 9 (2009).

<sup>5</sup>N. Ye and D. Y. Tang, J. Cryst. Growth **293**, 233 (2006).

<sup>6</sup>C. D. McMillen and J. W. Kolis, J. Cryst. Growth 310, 2033 (2008).

<sup>7</sup>J. Q. Yu, L. J. Liu, X. Y. Wang, H. T. Zhou, C. L. Zhang, and C. T. Chen, J. Cryst. Growth. **318**, 621 (2011).

<sup>8</sup>L. Mei, X. Huang, Y. Wang, Q. Wu, B. C. Wu, and C. T. Chen, Z. Kristallogr. 210, 93 (1995).

<sup>9</sup>Z. S. Lin, Z. Z. Wang, C. T. Chen, S. K. Chen, and M. H. Lee, Chem. Phys. Lett. **367**, 523 (2003).

<sup>10</sup>C. T. Chen, Z. S. Lin, and Z. Z. Wang, Appl. Phys. B **80**, 1 (2005).

<sup>11</sup>M. C. Payne, M. P. Teter, D. C. Allan, T. A. Arias, and J. D. Joannopoulos, Rev. Mod. Phys. **64**, 1045 (1992).

<sup>12</sup>S. J. Clark, M. D. Segall, C. J. Pickard, P. J. Hasnip, M. J. Probert, K. Refson, and M. C. Payne, Z. Kristallogr. 220, 567 (2005).

<sup>13</sup>D. Vanderbilt, Phys. Rev. B **41**, 7892 (1990).

<sup>14</sup>J. P. Perdew, K. Burke, and M. Ernzerhof, Phys. Rev. Lett. 77, 3865 (1996).

<sup>15</sup>H. J. Monkhorst and J. D. Pack, Phys. Rev. B **13**, 5188 (1976).

<sup>16</sup>T. H. Fischer and J. Almlof, J. Phys. Chem. **96**, 9768 (1992).

<sup>17</sup>L. J. Liu, X. Y. Wang, J. Q. Yu, and C. T. Chen (To be submitted).

<sup>18</sup>T. A. Halgren and W. N. Lipscomb, Chem. Phys. Lett. **49**, 225 (1977).

<sup>19</sup>J. V. Barth, G. Costantini, and K. Kern, Nature **437**, 671 (2005).

<sup>20</sup>C. T. Chen, in *Laser Science and Technology, An International Handbook*, Vol.15, edited by V. S. Letokhov, C. V. Shank, Y. R. Shen, and H. Walther (Harwood, Chur, Switzerland, 1993).